

Impurity transport driven by electrostatic turbulence in tokamak plasmas

T. Fülöp 1), S. Braun 2), I. Pusztai 1)

1) Nuclear Engineering, Department of Applied Physics, Chalmers University of Technology and Euratom-VR Association, Göteborg, Sweden

2) Max-Planck-Institut für Plasmaphysik, Greifswald, Germany

e-mail contact of main author: tunde@chalmers.se

Abstract. Impurity transport driven by electrostatic turbulence is analyzed in weakly-collisional tokamak plasmas using a semi-analytical model based on a boundary-layer solution of the gyrokinetic (GK) equation. Analytical expressions for the perturbed density responses are derived and used to calculate the stability boundaries, mode frequencies, growth rates and the quasilinear particle fluxes. Parametric dependencies of the above quantities with respect to impurity charge Z , effective charge Z_{eff} , impurity density scale length L_{nz} , and collisionality, and the effect of the impurities on the stability boundaries, have been determined and compared with quasilinear GK simulations with GYRO resulting in very good agreement. An analytical approximate expression of the zero-flux impurity density gradient is derived and used to discuss its parametric dependencies.

Introduction Understanding impurity transport in tokamak plasmas is important since fusion performance is significantly affected by impurities. To get reliable predictions for the turbulent fluxes, nonlinear electromagnetic GK simulations are needed, but these are costly in computing time. However, the quasilinear electrostatic approximation has been proven to retain much of the relevant physics and reproduce the results of nonlinear GK simulations for a wide range of parameters [1]. Reduced theoretical models, based on quasilinear approximations, benchmarked to GK simulations can ease the interpretation of the results of experiments or numerical simulations and can contribute to the better understanding of the underlying processes.

Model The aim of the present work is to calculate the quasilinear Gyrokinetic Impurity transport driven by ElectroStatic turbulence (GYIMES) using a semi-analytical model based on a boundary layer solution of the GK equation. The model does not rely on expansions in the smallness of the magnetic drift frequencies, and includes collisions modelled by a Lorentz operator. Following the approach of Ref. [2,3], we use a model electrostatic potential $\phi(\theta) = \phi_0 [(1 + \cos \theta)/2 + i f_s \sin^2 \theta] [H(\theta + \pi) - H(\theta - \pi)]$, where H is the Heaviside function, $f_s = -0.6s + s^2 - 0.3s^3$, s is the magnetic shear and θ is the ballooning angle. This model potential is motivated by variational analysis and GK simulations. By assuming large aspect-ratio, low beta, toroidal symmetry, circular cross section and weak collisionality, analytical expressions can be derived for the ion, impurity

and electron perturbed densities. The quasi-neutrality equation is solved numerically to obtain the frequencies and growth rates of the unstable modes, including the effect of impurities on these modes, and the quasilinear impurity particle fluxes. In this paper, we study only ion-temperature-gradient (ITG) turbulence dominated cases, but the model is suitable for trapped-electron mode turbulence as well. Using the analytically calculated expression for the perturbed impurity density response, we derive an approximate expression for the zero-flux impurity density gradient (the so-called peaking factor). Such a zero impurity flux region is relevant to steady state plasmas in the core of tokamaks since the impurity influx occurs through the edge.

Perturbed density responses The perturbed electron, ion and impurity responses are obtained from the linearized GK equation. We assume the following ordering of the electron/ion bounce frequencies and the eigenfrequency of the mode, $\omega_{bi} \ll \omega \ll \omega_{be}$, and consider weakly-collisional plasmas so that $\nu_{*e} = \nu_e/\epsilon\omega_{be} \ll 1$, where $\epsilon = r/R$ and ν_e is the electron collision frequency. Expanding the perturbed electron distribution as $\hat{g}_e = g_{e0} + g_{e1} + \dots$ for $\nu_e/\epsilon\omega_{be} \ll 1$ and $\omega/\omega_{be} \ll 1$ we find that the electron GK equation can be written as

$$(\omega - \langle\omega_{De}\rangle)g_{e0} - \frac{i\nu_e}{\epsilon K(\kappa)} \frac{\partial}{\partial \kappa} \hat{J}(\kappa) \frac{\partial g_{e0}}{\partial \kappa} = -\frac{e\langle\phi\rangle}{T_e} (\omega - \omega_{*e}^T) f_{e0}, \quad (1)$$

where $\kappa = [1 - \lambda B_0(1 - \epsilon)] / (2\epsilon\lambda B_0)$ is the trapping parameter, $\omega_{*a}^T = \omega_{*a} [1 + (x_a^2 - \frac{3}{2})\eta_a]$, $\omega_{*a} = -k_\theta T_a / e_a B L_{na}$ is the diamagnetic frequency, k_θ is the poloidal wave-number, $x_a = v/v_{Ta}$, $v_{Ta} = (2T_a/m_a)^{1/2}$, $\eta_a = L_{na}/L_{Ta}$, $L_{na} = -[\partial(\ln n_a)/\partial r]^{-1}$, $L_{Ta} = -[\partial(\ln T_a)/\partial r]^{-1}$, $\hat{J} = E(\kappa) + (\kappa - 1)K(\kappa)$, $E(\kappa)$ and $K(\kappa)$ are the complete elliptic integrals. The bounce-average of the potential is

$$\langle\phi\rangle = \phi_0 \{E(\kappa)/K(\kappa) + i(4f_s/3) [(2\kappa - 1)E(\kappa)/K(\kappa) + 1 - \kappa]\},$$

and the orbit-averaged precession frequency for trapped electrons is

$$\langle\omega_{De}\rangle = \omega_{D0} [E(\kappa)/K(\kappa) - 1/2 + 2s(E(\kappa)/K(\kappa) + \kappa - 1)],$$

where $\omega_{D0} = -k_\theta v^2 / \omega_{ce} R$ and $\omega_{ca} = e_a B / m_a$ is the cyclotron frequency. The second term on the left of Eq. (1) represents the Lorentz collision operator.

In the limit of small collisionalities, we can construct a boundary layer solution to Eq. (1) which reads

$$g_{e0} = g_{outer} \left(1 - \exp \left[-(1 - \kappa) \sqrt{\hat{u}K(\kappa)/\hat{v}} \right] \right), \quad (2)$$

where $\hat{u} = -i(y - \langle \omega_{De} \rangle / \omega_0)$, $\hat{v} = v_e / \omega_0 \epsilon$, $\omega_0 = |\Re\{\omega\}|$, $y = \omega / \omega_0$ and

$$g_{outer} = \frac{e \langle \phi \rangle (\omega_{*e}^T - \omega) f_{e0}}{T_e (\omega - \langle \omega_{De} \rangle)}. \quad (3)$$

To make analytical progress we will approximate the elliptic integral in the exponent of g_{e0} with a constant value $K(\kappa) \simeq \int_0^1 K(\kappa) d\kappa = 2$. Interestingly, the boundary layer solution (2) is a very good approximation of the numerically obtained distribution function g_{e0} even when \hat{v} is of order unity. Figure 1 shows the absolute value of the trapped electron distribution function as a function of the trapping parameter κ for various \hat{v} and $f_s = 0.18$, $y = -1 + 0.2i$ and $\tilde{\omega}_D = 0.6$. Solid (black) line is the numerical solution of Eq. (1), dashed (red) line is the boundary layer solution from Eq. (2) using a constant approximation for $K(\kappa) = 2$ in the exponent.

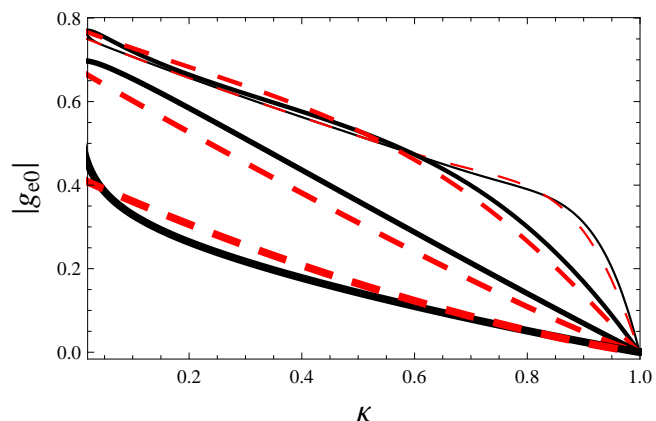


Figure 1: *Boundary layer and numerical solutions for $|g_{e0}|$ as function of κ . The lines correspond to $\hat{v} = 0.01, 0.1, 1, 5$ (from thinner to thicker).*

The perturbed electron response is proportional to $\langle \int g_{e0} d^3v \rangle = 4\sqrt{2}\epsilon \int_0^\infty v^2 dv \int_0^1 K(\kappa) g_{e0} d\kappa$, where, using the solution from Eq. (2) and the identity

$$\int_0^1 \left\{ E(\kappa) + i \frac{4f_s}{3} [(2\kappa - 1)E(\kappa) + (1 - \kappa)K(\kappa)] \right\} d\kappa = \frac{4}{3} \left(1 + i \frac{4f_s}{5} \right),$$

the κ -integral can be evaluated. Performing the velocity-space integration, the perturbed electron density response becomes

$$\frac{\hat{n}_e}{n_e} \frac{e\phi}{T_e} = 1 - \tilde{\phi} \left\{ \sqrt{2\epsilon} \left[\hat{\omega}_{\eta*e} - \frac{3}{2} \left(\eta_e \tilde{\omega}_{*e} - \frac{\tilde{\omega}_{Dt}}{2} \hat{\omega}_{\eta*e} \right) \mathcal{F}_{5/2}^1 \left(\frac{\tilde{\omega}_{Dt}}{2} \right) \right] - \frac{\Gamma(\frac{3}{4}) \sqrt{\epsilon \hat{v}_t}}{\sqrt{-i\pi y}} \left[2\hat{\omega}_{\eta*e} \mathcal{F}_{3/4}^{3/2} \left(\frac{\tilde{\omega}_{Dt}}{2} \right) - \frac{3\eta_e \tilde{\omega}_{*e}}{2} \mathcal{F}_{7/4}^{3/2} \left(\frac{\tilde{\omega}_{Dt}}{2} \right) \right] \right\}, \quad (4)$$

where $\tilde{\phi} = (1 + 4if_s/5)4\phi_0/(3\pi\phi)$, $\tilde{\omega}_{Dt} = \omega_{D0}/(\omega x_e^2)$, $\hat{v}_t = \hat{v} x_e^3$, $\tilde{\omega}_{*a} = \omega_{*a}/\omega$, $\hat{\omega}_{\eta*a} = 1 - (1 - 3\eta_a/2)\tilde{\omega}_{*a}$ and $\mathcal{F}_b^a(z) = {}_2F_0(a, b; ; z)$, where ${}_2F_0$ is the generalized hypergeometric function. $\mathcal{F}_b^a(z)$ incorporates the full effect of the drift resonances.

For the ions, we neglect the parallel compressibility by assuming $k_{\parallel} v_{Ti} \ll \omega$. In this limit, the GK equation can be solved neglecting the parallel derivative and replacing the magnetic drift frequency ω_{Di} with its weighted flux-surface averaged value $\langle \omega_{Di} \rangle_\phi$, where

$\langle X(\theta) \rangle_\phi = \int_{-\pi}^{\pi} X(\theta)\phi(\theta)d\theta / \int_{-\pi}^{\pi} \phi(\theta)d\theta$. Then the perturbed ion density becomes

$$\frac{\hat{n}_i}{n_i} \frac{e\phi}{T_i} = -\tilde{\omega}_{*i} + \left(\frac{3\tilde{\omega}_{Dsi}}{2} - b_i \right) \left[\hat{\omega}_{\eta^*i} - \frac{5}{2} (\eta_i \tilde{\omega}_{*i} - \tilde{\omega}_{Dsi} \hat{\omega}_{\eta^*i}) \mathcal{F}_{7/2}^1(\tilde{\omega}_{Dsi}) \right]. \quad (5)$$

Here, $b_a = \langle b_{sa} \rangle_\phi = b_{a0} [1 + s^2(2\pi^2 - 12 + if_s(2\pi^2 - 3))/(6(1 + if_s))]$ is the weighted flux-surface averaged value of the finite Larmor radius (FLR) parameter, $b_{sa} = b_{a0}(1 + s^2\theta^2)$, $b_{a0} = (k_\theta \rho_{sa})^2$ and $\rho_{sa} = v_{Ta}/\sqrt{2}\omega_{ca}$. Only the terms linear in b_{i0} were kept, an approximation that is typically valid for the fastest growing ITG modes ($k_\theta \rho_{si} \sim 0.2$). The averaged magnetic drift frequency is $\tilde{\omega}_{Dsa} = [6 + (9 + 16if_s)s\omega_{Da0}] / [12(1 + if_s)\omega]$, where $\omega_{Da0} = -2k_\theta v_{Ta}^2/3\omega_{ca}R$, and we used the constant energy resonance (CER) approximation for the ion resonance [$v_\perp^2 + 2v_\parallel^2 \rightarrow 4(v_\perp^2 + v_\parallel^2)/3$]. For impurities, if $(Z^3 m_e/m_i)^{1/2}(n_z Z^2/n_i)\epsilon\nu_{*e} \ll 1$, collisions can be neglected and we have

$$\frac{\hat{n}_z}{n_z} \frac{Ze\phi}{T_z} = -\tilde{\omega}_{*z} + \left(\frac{3\tilde{\omega}_{Dsz}}{2} - b_z \right) \left[\hat{\omega}_{\eta^*z} - \frac{5}{2} (\eta_z \tilde{\omega}_{*z} - \tilde{\omega}_{Dsz} \hat{\omega}_{\eta^*z}) \mathcal{F}_{7/2}^1(\tilde{\omega}_{Dsz}) \right]. \quad (6)$$

The dispersion relation follows from the quasi-neutrality condition $\hat{n}_e/n_e = (1 - Zf_z)\hat{n}_i/n_i + Zf_z\hat{n}_z/n_z$, where $f_z = n_z/n_e$ is the fraction of impurities.

Mode frequencies and growth rates Analyzing the dispersion relation, we find that for moderate or high charge number ($Z > 10$) the eigenfrequency and stability boundary are only weakly affected by increasing Z for constant Z_{eff} , and are approximately equal to the corresponding quantities in a pure plasma [3]. For lower Z , especially for helium or carbon dilutions, the effect of impurities influences the eigenfrequency and thus the stability boundary significantly. Figure 2 shows the Z and Z_{eff} -scalings of the normalized mode frequency and critical ion temperature gradient for marginal stability for the parameters $s = 1$, $q = 2$, $a/R = 1/3$, $a/r = 2$, $a/L_{ne} = 1$ and $k_\theta \rho_s = 0.2$.

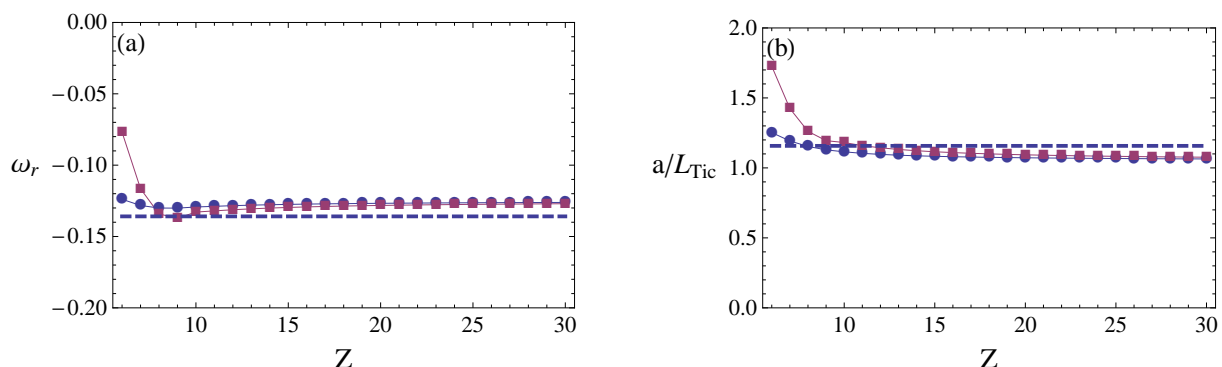


Figure 2: (a): Normalized mode frequency (in units of c_s/a) vs. Z (b): Critical ion temperature gradient vs. Z . Dashed: analytical expression from [3]. Dots: $Z_{\text{eff}} = 1.5$; squares: $Z_{\text{eff}} = 2$.

If the mode is far from marginal stability, the effect of increasing charge number affects the growth rates and mode frequencies only weakly, see Fig. 3a. The main reason for this

is the fact that the imaginary part of the impurity hypergeometric function is negligible compared with the ion term for $Z \gtrsim 10$. Figure 3b shows that the absolute values of the eigenfrequencies and growth rates decrease with increasing Z_{eff} , reflecting the fact that the impurity terms of the dispersion relation start to play a larger role when the impurity density is increased, and the presence of impurities is stabilizing.

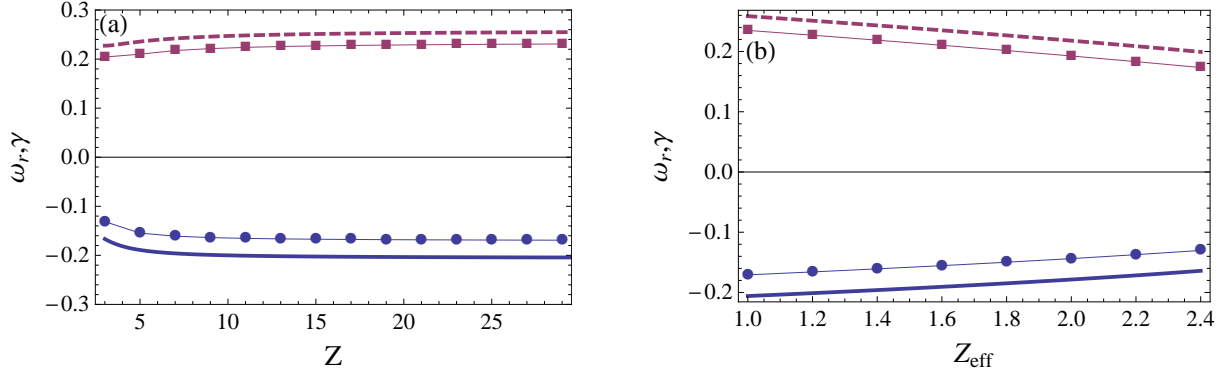


Figure 3: Mode frequency (solid) and growth rate (dashed) (in units of c_s/a) (a) $Z_{\text{eff}} = 1.5$; (b) $Z = 6$. The other parameters are $a/L_{Te} = a/L_{Ti} = 3$, $s = 1$, $q = 2$, $a/R = 1/3$, $r/a = 1/2$, $a/L_{ne} = 1$ and $k_{\theta}\rho_s = 0.2$ (GA standard case [4]). The dots and squares are the corresponding GYRO results.

Impurity particle fluxes The quasilinear particle flux for species a is given by

$$\Gamma_a = -\frac{k_{\theta}p_a}{eB} \left| \frac{e_a\bar{\phi}}{T_a} \right|^2 \Im \left(\frac{\bar{\hat{n}}_a/n_a}{e_a\bar{\phi}/T_a} \right), \quad (7)$$

where the bar denotes flux-surface averaged quantities, $\bar{\phi} = (1 + if_s)\phi_0/2$ and \hat{n}_a/n_a is the nonadiabatic perturbed density response. The quasilinear fluxes are evaluated using the expressions for the perturbed electron, ion and impurity densities from (4), (5) and (6), respectively.

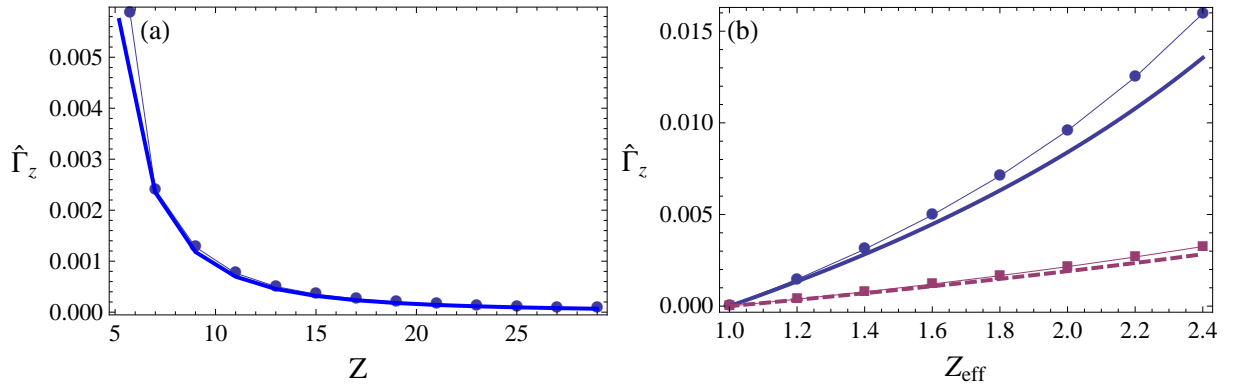


Figure 4: Impurity flux $\hat{\Gamma}_z$, normalized to $k_{\theta}p_e/eB |e\bar{\phi}/T_e|^2$, compared with linear GYRO results (dots) for the GA standard case. (a) $\hat{\Gamma}_z$ vs. Z for $Z_{\text{eff}} = 1.5$; (b) $\hat{\Gamma}_z$ vs. Z_{eff} for $Z = 6$ (solid), $Z = 10$ (dashed).

Solving the dispersion relation for the unstable frequencies and growth rate and calculating the normalized impurity flux from (7) we find that it is reduced with increasing charge number if Z_{eff} is kept constant, as shown in Fig. 4, although that is mainly due to the reducing impurity fraction $n_z/n_e \sim 1/Z^2$. The normalized flux increases for increasing impurity density, and this is more pronounced for impurities with lower Z since the relative increase in Z_{eff} is larger than for high Z .

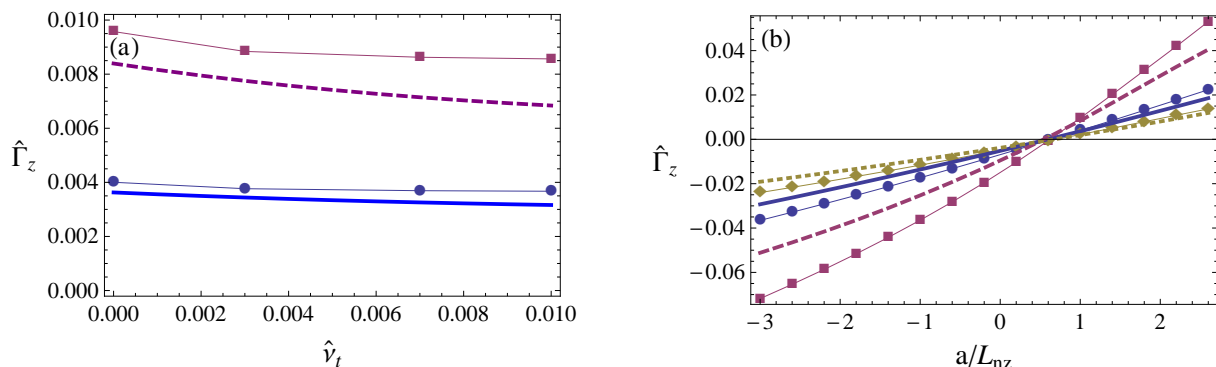


Figure 5: Normalized impurity flux $\hat{\Gamma}_z$ compared with linear GYRO results (dots) for the GA standard case. (a): $\hat{\Gamma}_z$ vs. normalized collisionality (in c_s/a) for $Z = 6$ and (solid) $Z_{\text{eff}} = 1.5$, (dashed) $Z_{\text{eff}} = 2$; (b): $\hat{\Gamma}_z$ vs. inverse radial impurity density gradient for the parameters: solid $Z_{\text{eff}} = 1.5$, $Z = 6$, dashed: $Z_{\text{eff}} = 2$, $Z = 6$, dotted: $Z_{\text{eff}} = 2$, $Z = 10$.

Collisions do not affect the mode frequencies, growth rates and impurity fluxes (see Fig. 5a) significantly. This is in contrast to the very sensitive dependence of the *electron* particle flux on collisionality, for which in general a sign change from inward to outward is expected at very small collisionalities. We note that the impurity flux changes sign at approximately the same value of R/L_{nz} , as shown in Fig. 5b, independently of Z , Z_{eff} and many other plasma parameters.

Peaking factor Using the analytically calculated expression for the perturbed impurity density response, it is possible to derive an approximative expression for the zero-flux impurity density gradient. Noting that the impurity hypergeometric function can be replaced by its asymptotic limit for small arguments, $\mathcal{F}_{7/2}^1(\tilde{\omega}_{Dsz}) = 1$ (which is a good approximation for heavy impurities since the argument $\tilde{\omega}_{Dsz} \propto 1/Z$) and furthermore assuming that the impurity FLR-term is negligible, $b_z \ll 3\tilde{\omega}_{Dsz}/2$, the zero-flux condition becomes

$$\Im \tilde{\omega}_{*z} = \Im \left\{ \frac{3\tilde{\omega}_{Dsz}}{2} \left[\hat{\omega}_{\eta*z} - \frac{5}{2} (\eta_z \tilde{\omega}_{*z} - \tilde{\omega}_{Dsz} \hat{\omega}_{\eta*z}) \right] \right\}. \quad (8)$$

From this we find that the expression for the zero-flux impurity density gradient is

$$\frac{R}{L_{nz}} = \frac{(2+3s)}{2} \frac{1 - \frac{2}{1+\hat{\gamma}^2} \frac{k_\theta \rho_s}{Z \tau_z \omega_0^n} \left(\frac{R}{L_{Tz}} - \frac{(2+3s)5}{6} \right)}{1 + \frac{2+3s}{1+\hat{\gamma}^2} \frac{k_\theta \rho_s}{Z \tau_z \omega_0^n}} \quad (9)$$

where we neglected terms of order $1/Z^3$ in the expression of the impurity flux and used the approximation $\tilde{\omega}_{Dsz} \simeq (2 + 3s)\omega_{Di0}/4\omega$ (valid if $f_s \ll 1$). Here, $\hat{\gamma} = \gamma/\omega_0$ is the normalized growth rate, ω_0^n is the absolute value of the eigenfrequency in units of c_s/R , k_θ is the poloidal wave-number of the most unstable wave, ρ_s is the ion sound radius, $\tau_z = T_e/T_z$ is the electron-impurity temperature ratio, and a and R are the minor and major radii of the torus.

The zero-flux impurity density gradient R/L_{nzc} is rather insensitive to Z and Z_{eff} for moderate or high Z , as been noted previously in quasilinear fluid simulations [5]. The reason is that the convective flux originating from the curvature drift is nearly independent of Z , while the convection caused by thermodiffusion decreases with increasing Z . For higher impurity temperature gradient or higher $k_\theta\rho_s$ the zero-flux impurity density gradient is lower, a trend which is in good agreement with numerical results. If, for instance, the inverse electron density scale length a/L_{ne} or the temperature ratio $\tau_i = T_e/T_i$ are changed, the unstable mode frequencies and growth rates will also change and R/L_{nzc} will be affected by that, especially for low Z when the effect of thermodiffusion cannot be neglected. This means that in scenarios with more peaked electron density profiles or strongly differing τ_i , R/L_{nzc} is expected to be different from that in scenarios with flat density profiles.

Figure 6 shows the peaking factor as function of charge number from Eq.(9), together with the results of linear GYRO simulations. For the parameters given in the caption of Fig. 6, the normalized frequency is $\omega_0^n \approx 0.86$ and growth rate $\hat{\gamma} \approx 0.44$ for adiabatic electrons and $\omega_0^n \approx 0.81$ and $\hat{\gamma} \approx 0.4$ for kinetic electrons (note that ω_0^n is normalized to c_s/R). The slight Z -dependence of the eigenvalues and the difference between the eigenvalues for adiabatic and kinetic electrons, does not have much effect on the analytical expression for the peaking factor given in Eq.(9). The solid line of Fig. 6 is the expression given

in Eq. (9) for $\omega_0^n \approx 0.86$, $\hat{\gamma} \approx 0.44$. As expected, the peaking factor increases with Z and saturates for high Z . This is in agreement with experimental trends for high- Z impurities and is due to the fact that for high Z , the effect of thermodiffusion is less important and the peaking factor is determined by the balance of curvature drift and diffusion.

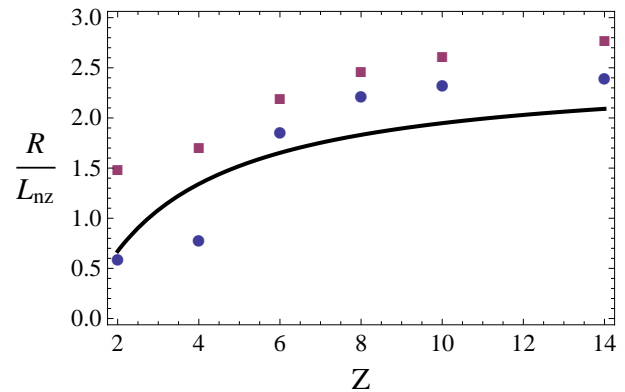


Figure 6: Zero-flux impurity gradient as function of Z from Eq. (9), together with linear GYRO results (dots for adiabatic electrons, squares for kinetic electrons) for the parameters: $s = 1$, $q = 2$, $a/R = 1/3$, $a/r = 2$, $a/L_{ni} = 1$, $a/L_{Ti} = a/L_{Te} = a/L_{Tz} = 2$, $\tau_z = 1$, $Z_{\text{eff}} = 1.01$ and $k_\theta\rho_s = 0.3$.

Conclusions In this paper we presented a semi-analytical model for impurity transport driven by electrostatic turbulence. The model does not rely on expansions in the smallness of the magnetic drift frequencies, and includes electron-ion collisions modeled by a Lorentz operator. The results agree well with linear gyrokinetic simulations with GYRO. It includes some effects that previously have been neglected in analytical calculations, for instance collisions and magnetic drifts are treated with more accuracy than in other, existing semi-analytical models, but it is still simple enough to ease the interpretation of certain physical effects, as we illustrated with the approximation for the zero-flux impurity density gradient. Because of its simplicity, it is straightforward to extend it by including several impurity species or include it in transport simulations. However, due to the model electrostatic potential used in the calculations, reliable quantitative predictions can only be obtained in the moderate shear region.

Acknowledgements This work was funded by the European Communities under Association Contract between EURATOM, Germany and *Vetenskapsrådet*. The views and opinions expressed herein do not necessarily reflect those of the European Commission. The authors would like to thank J. Candy for providing the GYRO code and H. Nordman for fruitful discussions.

References

- [1] A. CASATI et al, Nucl. Fusion **49**, 085012 (2009).
- [2] T. FÜLÖP, S. BRAUN, I. PUSZTAI, Phys. Plasmas **17**, 062501 (2010).
- [3] I. PUSZTAI, T. FÜLÖP, J. CANDY, J. R. HASTIE, Phys. Plasmas **16**, 072305 (2009).
- [4] R. E. WALTZ, J. CANDY, M. FAHEY, Phys. Plasmas **14**, 056116 (2007).
- [5] T. FÜLÖP, H. NORDMAN, Phys. of Plasmas **16**, 032306 (2009).